CrystEngComm

Accepted Manuscript

ROYAL SOCIETY OF CHEMISTRY

www.rsc.org/crystengcomm

Two-step vapor transport deposition of large-size bridge-like Bi_2Se_3 nanostructures

Manshu Han, Jiangang Ma,* Haiyang Xu** and Yichun Liu

Centre for Advanced Optoelectronic Functional Materials Research and Key Laboratory for UV Light-Emitting Materials and Technology of Ministry of Education, Northeast Normal University, Changchun 130024, China

Abstract

In this paper, single crystalline Bi_2Se_3 nanostructures including nanowires, nanoribbons, nanoplates and bridge-like nanostructures have been grown by physical vapor deposition. By investigating the morphological evolution of the Bi_2Se_3 nanostructures, we found that Bi_2Se_3 nanoribbons with the long axis along $<11\bar{2}0>$ could facilitate the formation of bridge-like nanostructures. Subsequently, a two-step growth process had been developed to increase both the size and the amount of the bridge-like Bi_2Se_3 nanostructures effectively, which shows great promise to realize the growth of large-size two dimensional materials for various optoelectronic and spintronic applications.

*Corresponding authors
*E-mail: majg@nenu.edu.cn; Fax: 85099772; Tel: +86 431 85099767
**E-mail: hyxu@nenu.edu.cn; Fax: 85099772; Tel: +86 431 85099767

Introduction

In the past few years, two dimensional (2D) layered materials such as graphene, BN, Bi_2Te_3, Bi_2Se_3, WS_2 and MoS_2 have been of great interest to scientists due to their novel physical and chemical properties and various potential applications in optoelectronics, spintronics, catalysis, energy storage and so on.[1-3] Bi_2Se_3, a former thermoelectric and infrared detecting material, now has been recognized as a typical topological insulator material with a large nontrivial bulk gap of ~0.3 eV and the simplest single-Dirac-cone surface state at the Γ point (refer to the origin of Brillouin zone). The crystal structure of Bi_2Se_3 is rhombohedral with five atoms in one unit cell. The lattice parameters of the hexagonal cells of Bi_2Se_3 are 0.4140 nm and 2.8636 nm for the a- and c-axes, respectively, and the conventional unit cell spans over three quintuple layers (QLs).[4-6] Therefore, each QL consists of five monoatomic planes as Se-Bi-Se-Bi-Se stacking along the c-axis. The atomic arrangement of the conventional unit cell is visualized in terms of the layered structure, as shown in Fig. 1. The strong spin-orbit coupling in layered Bi_2Se_3 dictates robust surface states, which are topologically protected against back scattering from time-reversal invariant defects and impurities. It has been observed that the band gap of a single QL Bi_2Se_3 is larger than that of multiple-QLs because the latter has less coupling between the surface states of the top and bottom interfaces.[7]

In a single Bi_2Se_3 QL, Se and Bi ions were bonded together by covalent bonds. However, single QLs are weakly bound to one another via the Van der Waals forces. As a result, mono- or multiple-layer materials can be obtained directly by mechanical exfoliating,[8] supersonic exfoliation[1] and laser exfoliation[9] from bulk Bi_2Se_3 powders. However, the dimension of the layered Bi_2Se_3 is dependent on the size of the bulk material and is generally less than ten microns. So far, some synthetic methods including sonochemical methods[10], solvothermal synthesis[11] have also been exploited to synthesize layered Bi_2Se_3 materials with the dimension up to twenty microns. However, these chemical methods will inevitably give rise to surface contaminations which have severe impacts on the characteristics of the topological insulating surface states. On the other hand, single and multiple Bi_2Se_3 QLs can be fabricated by some state-of-art techniques like molecular beam epitaxy (MBE) and metal-organic chemical vapor deposition (MOCVD). [12] For example, Q. K. Xue and his coworkers had grown single crystalline Bi_2Se_3 QLs with the thicknesses of just a few nanometers by MBE and demonstrated the topological insulator characteristic in ultrathin QLs.[13] However, it is still challenging to precisely control the dimension and the thickness of Bi_2Se_3 QLs in large scale.

Physical vapor deposition (PVD), typically including the vapor-solid (VS) and vapor-liquid-solid (VLS) mechanisms, is a conventional method

to obtain various single-crystalline nanostructures with large dimensions and diverse morphologies.[4, 14, 15] Compared to the CVD method, Bi_2Se_3 nanostructures grown by PVD generally have good enough crystalline quality that can suppress the carrier density in the bulk and facilitate the observation of the topological conducting surface states.[16]

In this paper, we will report the synthesis of various Bi_2Se_3 nanostructures such as nanowires (NWs), nanoribbons (NRs), nanoplates (NPs) and bridge-like nanostructures by VS and VLS growth processes. Noteworthy, we have developed a two-step growth process for increasing the size and the amount of the bridge-like Bi_2Se_3 nanostructures. Our studies provide a new way to prepare 2D Bi_2Se_3 multiple QLs with the size up to several tens of microns, which is critical for the fundamental researches and the potential applications of layered Bi_2Se_3.

Experiments

Growths of Bi_2Se_3 nanostructures were conducted with a vacuum tube furnace equipped with a 30 mm diameter quartz tube. The temperature profile of the furnace is shown in Fig. 2. The source material, Bi_2Se_3 powder (5N, 0.2g per growth)，is placed at the center of the furnace. In a typical synthesis process, the tube was pumped down to a base pressure of 8×10^{-1} Pa by a mechanical pump and then was flushed with Ar gas several times to remove residual oxygen. 1x1 cm^2 sized Si/SiO_2 (001) substrates were placed on the downstream side of the

source. The furnace was heated up to 550 ^{o}C at a rate of 5 ^{o}C/min. After that, Ar flow rate was fixed at 130 standard cubic centimeters (sccm) for 3 hours, and then the substrates were cooled down to room temperature naturally. At the end of growths, a gray layer is evidently observable by naked eyes on the substrates and the inside wall of quartz tube. To implement growths in VLS mechanism, 5~10 nm thick Au films were coated on the substrates by thermal evaporation as the catalyst.

The surface morphologies and crystalline structures of the as-deposited products were characterized by a FEI Quanta 250 field-emission scanning electron microscope (SEM), a Rigaku D/MAX 2500 PC automatic powder X-ray diffractometer (XRD), a Jobin Yvon HR800 micro-Raman spectroscopy, a 200 kV FEI Tecnai G^2 F20 transmission electron microscopy (TEM), an Olympus BX51 optical microscopy, and a Bruker multimode 8 atomic force microscopy (AFM) in the tapping mode.

Results and discussion

Firstly, Bi_2Se_3 nanostructures were synthesized though the VS mechanism. Figure 3 (a-g) show the SEM images of the samples placed at the temperatures zone of 540, 524, 510, 490, 460, 440, 415^{o}C, respectively. The corresponding positions away from the center of the heat source are shown in Fig. 2. As can be seen from Fig. 3 (a), at 540 ^{o}C, the substrate was covered by a mass of randomly oriented irregular

nanostructures. Some Bi_2Se_3 NWs and NRs with the diameter in the range of 100 to 500 nm and the length of more than ten microns stretched out from the edge of these irregular nanostructures. In general, the growth of 1D or 2D nanostructures by VS mechanism can be explicated by Frank's theory.[17-20] Without help of metal catalysts the adsorbed molecules coming from the sources will nucleate into tiny crystal seeds at low energy sites on the substrate surface once the nucleus reached the critical size. Then, various nanostructures will grow from the seeds. Mostly, well-faceted structures will be formed due to the difference of surface energies and surface migration velocities between different crystal faces.

As shown in Fig. 3(b-g), when the substrate temperature is 524 ^{o}C or lower, the substrate surface was covered by well-faceted hexagonal and triangular NPs whose sizes and thicknesses decreased with the decreasing temperature. In Fig. 3(b), a large number of hexagonal Bi_2Se_3 NPs with smooth surface and clear steps can be observed. The presence of steps indicates that the Bi_2Se_3 NPs were formed by layer-on-layer growth. When the temperature is 490 ^{o}C, the orientation of the NPs is uniform with the hexagonal planes parallel to the substrate surface, as shown in Fig. 3 (d). As the substrate temperature continues to decrease, the size of NPs shrinks and the shape of NPs changes from hexagonal to polygonal (shown in Fig. 3(e)). When the substrate temperature is 440 ^{o}C or lower,

only the triangular Bi_2Se_3 NPs with size of several tens of nanometers are observed, as shown in Fig. 3 (f) and (g). To confirm the microstructure of the synthesized Bi_2Se_3 nanostructures, some features shown in Fig. 3(e) were transferred to copper grid for TEM measurements. As shown in Fig. 3(h), an equilateral triangle NP with straight edges can be observed. The corresponding selected-area electron diffraction (SAED) pattern and the high resolution TEM (HRTEM) image taken at the red circle were shown as insets in Fig. 3(h). The spotty SAED pattern and the clear lattice fringes indicate that the NP has single crystal nature with each edge parallel to the $<11\bar{2}0>$ directions.

From the thermodynamic point of view, the anisotropic morphologies of nanostructures are determined by the relative surface energies of various crystal planes. The facets with lower surface energies will be favored and mostly exposed. As reported by Yan and his coworkers, [21] among the three low index planes {0001}, $\{10\bar{1}0\}$ and $\{11\bar{2}0\}$ of rhombohedral Bi_2Se_3, {0001} planes have the lowest surface energy (i.e. Gibbs's free energy), resulting in the 2D morphology of Bi_2Se_3. Meanwhile, $\{10\bar{1}0\}$ planes have lower surface energy than $\{11\bar{2}0\}$ planes. Therefore, we can conclude that the exposed facets of the triangle NP in Fig. 3(h) must belong to the $\{10\bar{1}0\}$ planes of Bi_2Se_3.

Figure 3 (i) shows EDAX analysis of the Bi_2Se_3 nanostructures. The average Bi/Se atomic ratio of the samples grown at different temperature

is 2.03/2.97, indicating that the Bi_2Se_3 nanostructures are very close to the stoichiometry. The large yield of materials allows us to collect enough materials for XRD measurements. The XRD measurements were conducted in a conventional θ/2θ scan type. The upper and lower curves in Fig. 3 (j) show the corresponding XRD patterns of the samples shown in Fig. 3 (b) and (e), respectively. All of the diffraction peaks match well with the standard data of the rhombohedral Bi_2Se_3. The full-width at half-maximum (FWHM) of the (006) peaks is only 0.17^o, indicating that Bi_2Se_3 nanostructures grown by VS mechanism have excellent crystallinity. It is noteworthy that only the c-axis diffraction peaks can be observed in the θ/2θ scan for the sample presented in Fig. 3 (e). Therefore, it can be concluded that the Bi_2Se_3 NPs in Fig. 3 (e) grow preferentially along in-plane directions with their c-axes perpendicular to the substrate surface.

Raman scattering measurements were carried out using a micro-Raman spectroscopy system with a 488 nm laser as excitation source. In Fig. 3 (k), the red and the black curves correspond to the Raman spectra of the same sample as in Fig. 3 (e) and the bulk Bi_2Se_3 powder, respectively. Two characteristic peaks at ~131 cm^{-1} and ~175 cm^{-1} correspond to the in-plane (E_g^2) and the out-of-plane vibration mode (A_{1g}^2) of the rhombohedral Bi_2Se_3 lattice, respectively, whose intensities are reported to be very sensitive to the thickness of NPs.[22] As can be seen

in Fig. 3 (k), both E_g^2 and A_{1g}^2 vibrations are significantly strong for the Bi_2Se_3 NPs in comparison with the bulk Bi_2Se_3 powder. Such kind enhancement of E_g^2 and A_{1g}^2 vibrations in few QLs Bi_2Se_3 and Bi_2Te_3 NPs, which had been tentatively ascribed to the Fabry-Perot interference in the Bi_2Se_3 and Bi_2Te_3 NPs, indicates that the thicknesses of the NPs in Fig. 3 (e) would be less than 16 QLs.[23]

The growth of Bi_2Se_3 nanostructures were also carried out in the VLS growth mode. The growth conditions are the same as the VS growth except Au catalyst being used. In VLS growths, Au catalysts can accelerate the collection of raw materials and subsequently the growth rate of nanostructures.[24, 25] Figure 4 (a-e) show the SEM images of the samples grown by VLS mode at 500, 440, 370, 340, 250 ^oC, respectively. In Fig. 4 (a), a large number of small hexagonal Bi_2Se_3 nanostructures can be observed on the substrate surface with Au nanoparticles locating at the top of each hexagonal nanostructure. The diameters of the spherical Au nanoparticles are in the range of 100~600 nm. When the temperature is 440 ^oC, NWs and NRs with the length up to a hundred microns were obtained, as shown in Fig. 4 (b). For example, a 200 nm wide and over 100 μm long NW and a 1 micron wide and 30 micron long NR are shown in Fig. 4 (f) and (g), respectively. On the tip of the NW and the NR Au nanoparticles can be observed. Additionally, the widths of NWs or NRs increase with the increasing size of the Au nanoparticles, which is

common for the VLS growth of nanostructures.[26] The angle between the two straight edges of the NR shown in Fig. 4 (g) is measured to be 120° which is consistent with the angle between the $\{11\bar{2}0\}$ planes of the rhombohedral Bi_2Se_3. In contrast to the smooth NW and NR shown in Fig. 4 (f) and (g), another type of Bi_2Se_3 NW with clear steps and facets on its sidewall is shown in Fig. 4(h). EDAX analysis on the tip of the NW confirms that the hemispherical feature at the tip of the NW is made of Au. Such kind faceted sidewalls have been widely observed on Si NW grown by the VLS mode.[26-28] Xu et al. have attributed the formation of Si NWs with faceted sidewalls to the diffusion of tiny Au nanoparticles to the sidewalls as NWs growing along the long axis.[29] Therefore, we would tentatively speculate that the same mechanism can be used to explicate the growth of Bi_2Se_3 NW in Fig. 4(h). When the substrate temperature is 370 °C and lower, the surface of substrates is covered by a big amount of Bi_2Se_3 NPs whose sizes decrease with decreasing temperature, as shown in Fig. 4 (c-e). These NPs have flat and smooth surfaces. XRD patterns of the NPs are similar with the lower curve in Fig. 3 (j), indicating that the c-axes NPs also perpendicular to the substrate surface. In contrast with the VS growths implemented at the same temperature, small triangular Bi_2Se_3 NPs are rarely observed, but a few large Bi_2Se_3 NPs with the lateral dimension up to 50 μm were obtained, as shown in Fig. 4 (i). The morphological difference between the VLS and the VS growth is

probably due to the higher growth rate of the nanostructures in the VLS mode than in the VS mode. Figure 4 (j) shows the TEM image of a Bi_2Se_3 NR similar to the NR in Fig. 4 (g). The corresponding HRTEM image and SAED patterns taken at the red circle are presented as insets. The clear and indexed hexagonally SAED patterns reveal that the NR has single crystalline nature and grows preferentially along the $<11\bar{2}0>$ direction. The lattice spacing is calculated to be 2.3 Å which is consistent with the d-space of $(11\bar{2}0)$ planes of the rhombohedral Bi_2Se_3.

The formation of various Bi_2Se_3 nanostructures by the VS and the VLS growth modes can be discussed from the thermodynamic point of view. As discussed before, {0001} and $\{11\bar{2}0\}$ planes of Bi_2Se_3 have the lowest and the highest surface energy, respectively. At the high temperature zones where is close to the Bi_2Se_3 powders, highly supersaturated BiSe and Se_2 vapor resulted in the high growth rates nanostructures. Therefore, a large amount of nanostructures with various shape like ribbons, zigzag, diamond and polygon can be observed for the VS growths, as shown in Fig. 3 (a). As the substrate temperature and the BiSe and Se_2 vapor pressure decreased, the growth rate decreased correspondingly. The surface adsorbed molecules will have more time to migrate on the low energy surface, resulting in the lateral growth of Bi_2Se_3 NPs along in-plane directions. Therefore, we can see the formation of lots of micron to nanometer-sized hexagonal Bi_2Se_3 NPs with the

decreasing substrate temperature in the VS growth mode, as shown in Fig. 3 (b-g).

However, the situation will be different for the VLS growth mode. If the substrate temperature is higher than 500 ^{o}C, most of adsorbed vapor molecules re-evaporated away from the substrate surface except at the site of Au particles. As a result, only small and low density hexagonal plates can be observed, as shown in Fig. 4 (a). With the decreasing substrate temperature, the molecule re-evaporation rate was depressed and large dimensional structure emerged. When the substrate temperature is lower than 500 ^{o}C, a large number of Bi_2Se_3 NRs were formed due to the lowered reaction energy at the interface between liquid Au catalyst and Bi_2Se_3, as shown in Fig. 4 (b). The formation of NRs with $(10\bar{1}0)$ edges and (0001) top surfaces is energetically favorable from the thermodynamic point of view. Once the substrate temperature is lower than 440 ^{o}C, the preferential growth along $<11\bar{2}0>$ direction was replaced by the random growth along diverse directions, which is probably due to the substrate temperature is below the eutectic temperature of the catalyst alloy.

It is noteworthy that some novel bridge-like nanostructures consisting of two NRs and one NP can be observed when the substrate temperature in the range of 440~450 ^{o}C. Figure 5 (a) and (b) show the SEM image of a typical bridge-like nanostructure and the TEM image of

another one, respectively. In order to compare the lattice constants and the orientations of the NR and the NP, SAED and HRTEM measurements were conducted at the two red circles in Fig. 5 (b). The electron diffraction patterns and lattice fringes kept unchanged when the electron beam shift between these two spots, revealing that the NP and the NR have the same crystalline structure and orientation.

From a survey of the SEM images, we also notice that a large number of Bi_2Se_3 NRs and NPs were formed at high and low temperature zones, respectively. On the contrary, bridge-like nanostructures are rare and only appear at a specific medium temperature zone. In addition, most of the bridge-like nanostructures are suspended in midair with the NRs attaching to the substrate. Therefore, it is reasonable to speculate that the formation of the bridge-like nanostructures originate from the epitaxial growth of NPs on the sidewalls of NRs along one of the $<11\bar{2}0>$ directions. In order to obtain more bridge-like nanostructures with large dimension, we developed a two-step growth process in which NWs and NRs were utilized as the nucleation centers and templates for the subsequent lateral growths of NPs. The details of the two-step growth process can be briefly addressed as follows. Firstly, Bi_2Se_3 NWs and NRs were fabricated by the VLS growth at 475 ^{o}C for 120 minutes, and then the growth was paused. Secondly, the substrates were shifted 1 centimeter towards the downstream side where the temperature was 460 ^{o}C. Then the

growth was resumed for 120 minutes. The Ar flow rate was kept at 65 sccm during the first and the second step growths.

Figure 6 (a) and (b) show SEM images taken at the same area before and after the second step growth, respectively. As can be seen in Fig. 6 (c), some NWs with length up to one hundred microns can be observed after the first growth. After the second growth, many bridge-like nanostructures with lateral dimension larger than 30 microns are observed, as shown in Fig. 6 (d). A survey on the average size and the number of the bridge-like Bi_2Se_3 nanoplates has been done, which shows that the average size of bridge-like structure increased from 8 μm^2 for the conventional growth to 13.4 μm^2 for the two-step growth. More importantly, by employing the two step growth, the number of Bi_2Se_3 bridges with the size larger than 30μm^2 nearly increased by twenty times.

The formation of bridge-like structure in two-step growths can be understood by simply combining the VLS and the VS growth mechanisms discussed above. Briefly speaking, the contribution of the long Bi_2Se_3 NRs to the formation of Bi_2Se_3 bridges in the second step VS growth can be summarized in two aspects. First, the long NRs can offer more nucleation sites on their $(10\bar{1}0)$ edges, which can facilitate the in-plane growth of bridge deck. Second, the NRs will work as the original templates which limit the width and even the thickness of bridges.

To further prove our assumption about the formation of bridge-like

Bi_2Se_3 nanostructures, five NRs were mechanically transferred by a micro-probe station from the firstly grown sample onto a clean SiO_2 substrate, as shown in Fig. 7 (a). Then, the five NRs on the clean SiO_2 substrate were put into the furnace for the secondary growth with the same condition mentioned above. Figure 7 (b) and (c) show the surface morphology after the secondary growth by optical microscopy and SEM, respectively. It can be seen that after the secondary growth the lateral dimension of the NRs increase significantly from half or one micron to ten microns. While the heights of the NRs increase from 50~100 nm to ~1 micron which is estimated by defocus effects of the optical microscopy. However, for the central NR among the five NRs there are two positions where the width and the height did not change significantly. We labeled the two positions as 1 and 2 in Fig. 7 (b) and (c). The zoom-in optical microscopy and SEM images at the position 1 and 2 are shown in Fig. 7 (b_1-b_2) and (c_1-c_2). At the position 1, multiple steps of NPs with clear facets are connected by a narrow NR whose width is almost unchanged after the second growth. Obviously, these micron-sized NPs have been extending from the narrow NR with the upper NPs constraining to the bottom ones. At the position 2, a NP with uneven armchair-like edges is attached to the arc-shape NR. The contrast variation at the downside of the NP in Fig.7 (c_2) originates from the variation of thickness and will be discussed later. Additionally, the angles

between adjacent straight edges of the NPs shown in Fig.7 (c_1) and (c_2) are about 120°, which indicates that the top surface of the NPs and the NR is the {0001} plane of Bi_2Se_3, while the facets are the more stable $\{10\bar{1}0\}$ planes.

Figure 7 (d) and (e) show the AFM images taken at the position 1 and 2, respectively. In Fig. 7 (d), the uniform color contrast reveals that the top surface of the Bi_2Se_3 NPs and NR are atomic smooth. The height profile along the white dash line shows that the vertical and the horizontal dimensions of the NR are 64 nm and 480nm, respectively. While the step heights of the stacking NPs vary from several to tens of nanometers randomly, suggesting that the Bi_2Se_3 NPs are formed by layer-by-layer growth. In Fig. 7 (e), the height profiles along the white dash lines I and II reveal that the height and the width of the NR consist with that of the NR at the position 1. However, the height of the NP is uneven along the radial and the axial direction of the NR. The NP is 64nm thick at the near NR side and becomes thinner and thinner as the NP extending to the far-end side. However, the reason for the nonuniformity of height and width is not clear now. We tentatively ascribe it to the arc-shape of the NR at the position 2 in Fig. 7, because bending of NR might induce compressive strain accumulation and uneven growth rate in the Bi_2Se_3 NP. However, no exact explanation for the nonuniform growth rate at different portions of the single NR can be provided at this point. Further

studies have to be done to clarify the issue.

Conclusions

In summary, we report the synthesis of various Bi_2Se_3 nanostructures such as nanoribbons, nanoplates and bridge-like nanostructures by the VS and VLS growth mechanisms. Bi_2Se_3 nanoribbons with the growth normal along $<11\bar{2}0>$ directions are mostly formed at the high temperature zone. On the other hand, Bi_2Se_3 nanoplates with their c-axes perpendicular to the substrate surface are mainly formed by layer-by-layer growth at the low temperature zone. Meanwhile, novel bridge-like nanostructures generally consisting of two nanoribbons and one nanoplate are occasionally observed in a very narrow temperature window in the medium-temperature zone. In order to obtain more bridge-like nanostructures with large dimension, a two-step growth process has been developed to increase the number and the dimension of the bridge-like Bi_2Se_3 nanostructures, which provide an effective rout for fabricating large-size layered Bi_2Se_3 nanostructures and could benefit the fundamental researches and the optoelectronic and spintronic applications of topological insulators. The formation mechanism of various nanostructures was also discussed from the thermodynamic point of view.

Acknowledgements

The work is supported by the NSFC (Nos. 51172041, 51202026, 91233204, 51372035, 51422201 and 11204029), 973 Program (No. 2012CB933703), "111" project (No. B13013), the Fund from Jilin Province (Nos. 20121802, 201201061, 20140309012GX and 20140201008GX) and Doctoral Fund of Ministry of Education of China (No. 20110043120004), Fundamental Research Funds for the Central Universities (No. 2412015BJ003) and SKLLIM1404.

References

(1) V. Nicolosi, M. Chhowalla, M. G. Kanatzidis, M. S. Strano and J. N. Coleman, *Science*, 2013, **340**, 1419.

(2) F. Bonaccorso, L. Colombo, G. Yu, M. Stoller, V. Tozzini, A. C. Ferrari, R. S. Ruoff, V. Pellegrini, *Science*, 2015, **347**, 41.

(3) X. Huang, C. Tan, Z. Yin, H. Zhang, *Adv. Mater.*,2014, **26**, 1.

(4) D. Kong, J. C. Randel, H. Peng, J. J. Cha, S. Meister, K. Lai, Y. Chen, Z.-X. Shen, H. C. Manoharan and Y. Cui, *Nano Lett.*, 2010, **10**, 329-333.

(5) W. Dang, H. Peng, H. Li, P. Wang and Z. Liu, *Nano Lett.*, 2010, **10**, 2870-2876.

(6) H. Lind, S. Lidin and U. Häussermann, *Phys. Rev. B*, 2005, **72**, 184101.

(7) K. M. F. Shahil, M. Z. Hossain, V. Goyal and A. A. Balandin, *J. Appl. Phys.*, 2012, **111**, 054305.

(8) K. S. Novoselov, A. K. Geim, S. V. Morozov, D. Jiang, Y. Zhang, S. V. Dubonos, I. V. Grigorieva and A. A. Firsov, *Science*, 2004, **306**, 666-669.

(9) M. Qian, Y. S. Zhou, Y. Gao, J. B. Park, T. Feng, S. M. Huang, Z. Sun, L. Jiang and Y. F. Lu, *Appl. Phys. Lett.*, 2011, **98**, 173108.

(10) H. Cui, H. Liu, J. Wang, X. Li, F. Han and R. I. Boughton, *J. Cryst. Growth*, 2004, **271**, 456-461.

(11) G. Zhang, W. Wang, X. Lu and X. Li, *Cryst. Growth Des.*, 2009, **9**, 145-150.

(12) Y.-F. Lin, H.-W. Chang, S.-Y. Lu and C. W. Liu, *J. Phys. Chem. C*, 2007, **111**, 18538-18544.

(13) Y. Zhang, K. He, C.-Z. Chang, C.-L. Song, L.-L. Wang, X. Chen, J.-F. Jia, Z. Fang, X. Dai, W.-Y. Shan, S.-Q. Shen, Q. Niu, X.-L. Qi, S.-C. Zhang, X.-C. Ma and Q.-K. Xue, *Nat. Phys.*, 2010, **6**, 584-588.

(14) S. Wu, C. Huang, G. Aivazian, J. S. Ross, D. H. Cobden and X. Xu, *ACS Nano*, 2013, **7**, 2768–2772.

(15) M. Saghir, M. R. Lees, S. J. York and G. Balakrishnan, *Crys. Growth Des.*, 2014, **14**, 2009-2013.

(16) J. J. Cha, K. J. Koski and Y. Cui, *Phys. Status Solidi-R*, 2012, **1–11**.

(17) F. C. Frank, *Discuss. Faraday Soc.*, 1949, **5**, 48-54.

(18) F. C. Frank, S. P. F. Humphreys-Owen, I. N. Stranski, H. K. Hardy, W. K. Burton, N. Cabrera, R. S. Bradley, J. L. Amoròs, C. W. Bunn and U. R. Evans, *Discuss. Faraday Soc.*, 1949, **5**, 66-79.

(19) M. H. R. J. Plusjé, W. J. Dunning, W. K. Burton, N. Cabrera, R. F. Strickland-Constable, S. Fordham, F. C. Frank, W. E. Garner, K. G. Denbigh, W. A. Wooster, D. R. Hale, A. Juliard, A. E. Robinson, L. J. Griffin, I. N. Stranski, C. W. Bunn, Y. Haven, E. O. Hall, H. K. Hardy, H. E. E. Powers, A. F. Wells, A. R. Ubbelohde and J. L. Jones, *Discuss. Faraday Soc.*, 1949, **5**, 183-197.

(20) F. C. Frank, *Adv. Phys.*， 1952, **1**, 91-109.

(21) Y. Yan, Z.-M. Liao, Y.-B. Zhou, H.-C. Wu, Y.-Q. Bie, J.-J. Chen, J. Meng, X.-S. Wu, D.-P. Yu, *Sci. Rep.*, 2013, **3**, 1.

(22) J. Zhang, Z. Peng, A. Soni, Y. Zhao, Y. Xiong, B. Peng, J. Wang, M. S. Dresselhaus and Q. Xiong, *Nano Lett.*, 2011, **11**, 2407-2414.

(23) S. Y. F. Zhao, C. Beekman, L. J. Sandilands, J. E. J. Bashucky, D. Kwok, N. Lee, A. D. LaForge, S. W. Cheong and K. S. Burch, *Appl. Phys. Lett.*, 2011, **98**, 141911.

(24) R. S. Wagner and W. C. Ellis, *Appl. Phys. Lett.*, 1964, **4**, 89.

(25) R. S. Wagner, *in Whisker Technology, A. P. Levitt, Ed, (Wiley-Interscience, New York, 1970)*, 47-119.

(26) J. B. Hannon, S. Kodambaka, F. M. Ross and R. M. Tromp, *Nature*, 2006, **440**, 69-71.

(27) M. I. Hertog, J.-L. Rouviere, F. Dhalluin, P. J. Desre, P. Gentile, P. Ferret, F. Oehler and T. Baron, *Nano Lett.*, 2008, **8**, 1544-1550.

(28) T. Kawashima, T. Mizutani, T. Nakagawa, H. Torii, T. Saitoh, K. Komori and M. Fujii, *Nano Lett.*, 2008, **8**, 362-368.

(29) T. Xu, J. P. Nys, A. Addad, O. I. Lebedev, A. Urbieta, B. Salhi, M. Berthe, B. Grandidier and D. Stiévenard, *Phys. Rev. B*, 2010, **81**, 115403.

Figure captions

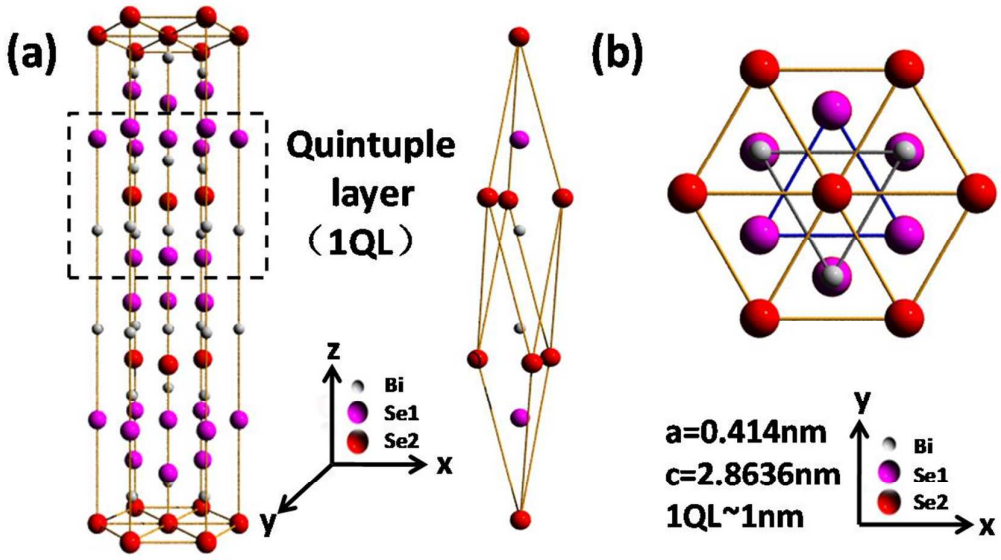

Figure 1. (a) Layered crystal structure of Bi_2Se_3, with each quintuple layer (QL) stacking in the Se-Bi-Se-Bi-Se sequence along the c axis, and a trigonal primitive cell of Bi_2Se_3. (b) Top-view of the schematic Bi_2Se_3 structure.

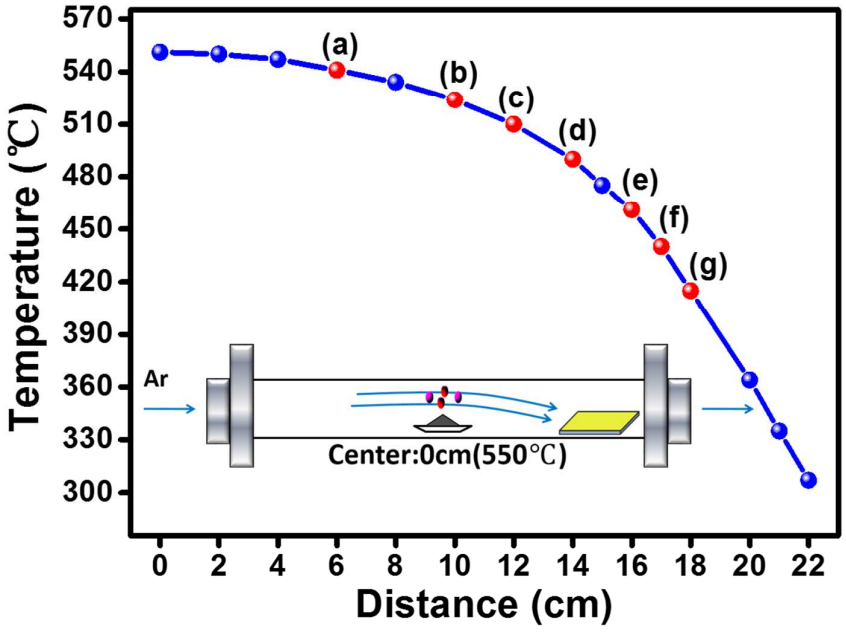

Figure 2. The temperature profile of the furnace (The zero point of the x-axis corresponds to the center of the furnace where Bi_2Se_3 sources were placed), the inset shows the schematic experimental setup.

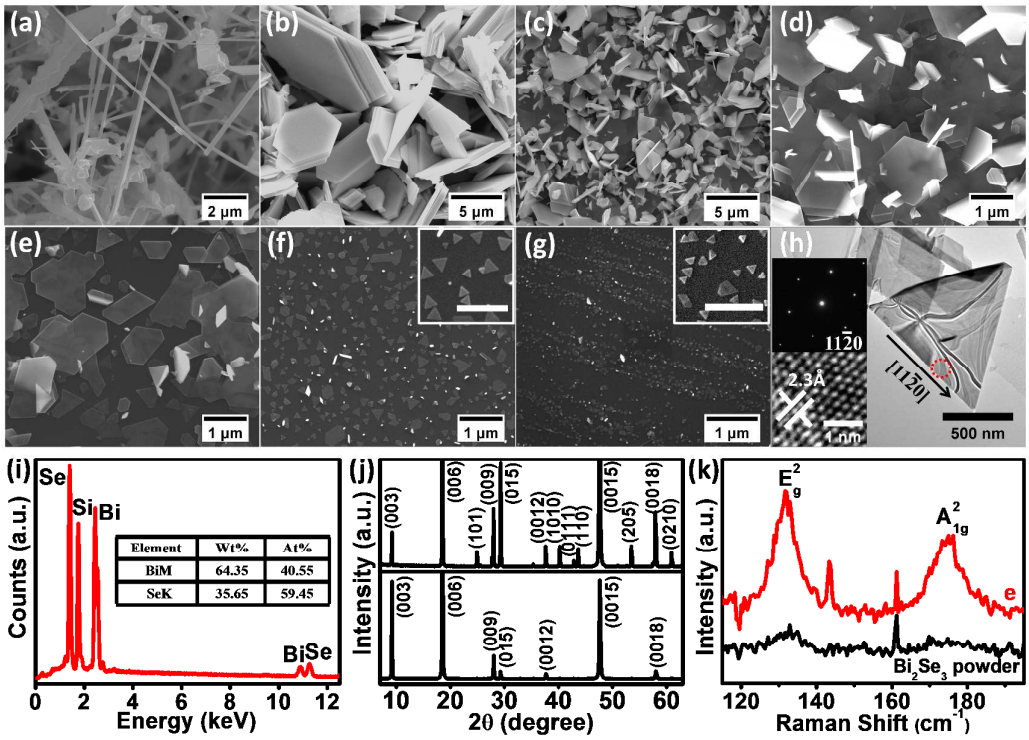

Figure 3. SEM images of Bi_2Se_3 nanomaterials synthesized by the VS mode. (a) Nanowires grown at 540 °C. (b)-(g) Bi_2Se_3 nanoplates grown at 524, 510, 490, 460, 440 and 415 °C, respectively. The scale bars of the insets are 500 nm. (h) TEM images of Bi_2Se_3 nanoplates. Insets are the corresponding HRTEM image and SAED patterns taken at the red circle. (i) EDAX analysis of the Bi_2Se_3 nanostructures. (j) θ-2θ scan X-ray diffraction of the samples grown at 524 °C (Upper) and 460 °C (Lower), respectively. (k) Raman spectra of the samples grown at 460 °C and bulk Bi_2Se_3 powder, respectively.

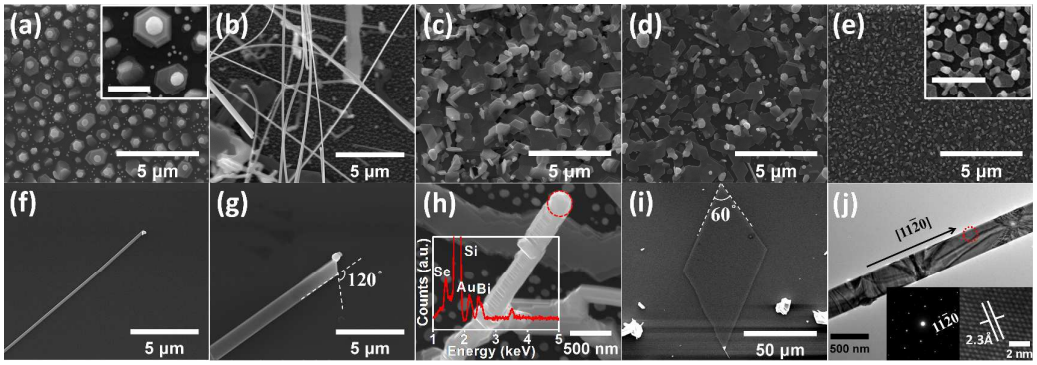

Figure 4. SEM images of Bi_2Se_3 nanomaterials synthesized by the VLS mode. (a) Hexagonal structures grown at 500 □. (b) Bi_2Se_3 nanowires grown at 440□. (c)-(e) Bi_2Se_3 nanoplates grown at 370, 340 and 250 □, respectively. The scale bars of the insets are 1μm. (f) A nanowire grown along c-axis. (g) A Sheet-like wide nanoribbon, the angle between the two straight edges of the nanoribbon is 120°. (h) A nanowire is formed by stacking of nanoplates. (i) A Large nanoplate. (j) TEM image of a Bi_2Se_3 nanoribbon. Insets are the corresponding HRTEM image and SAED patterns taken at the red circle.

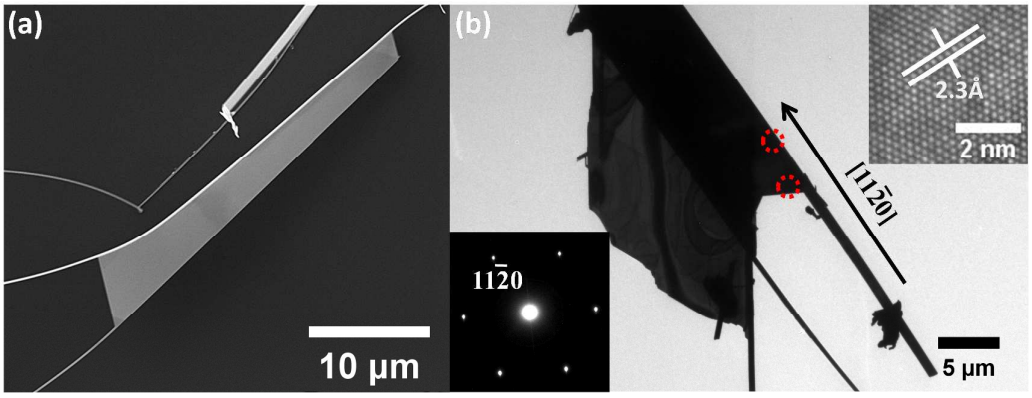

Figure 5. (a) Typical Bridge-like Bi_2Se_3 nanosturcture that consists of two nanoribbons and a nanoplate. (b) TEM image of a bridge-like Bi_2Se_3 nanostructure. Insets are the corresponding HRTEM image and SAED patterns taken at the red circles.

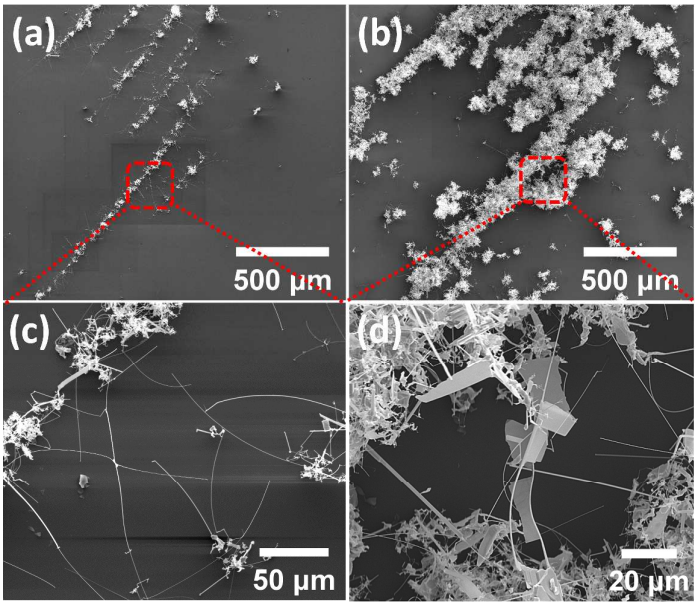

Figure 6. (a) and (b) are SEM images of Bi_2Se_3 nanostructures after the first time growth process and the secondary growth process, respectively. (c) and (d) are the corresponding zoom-in SEM images in (a) and (b), respectively.

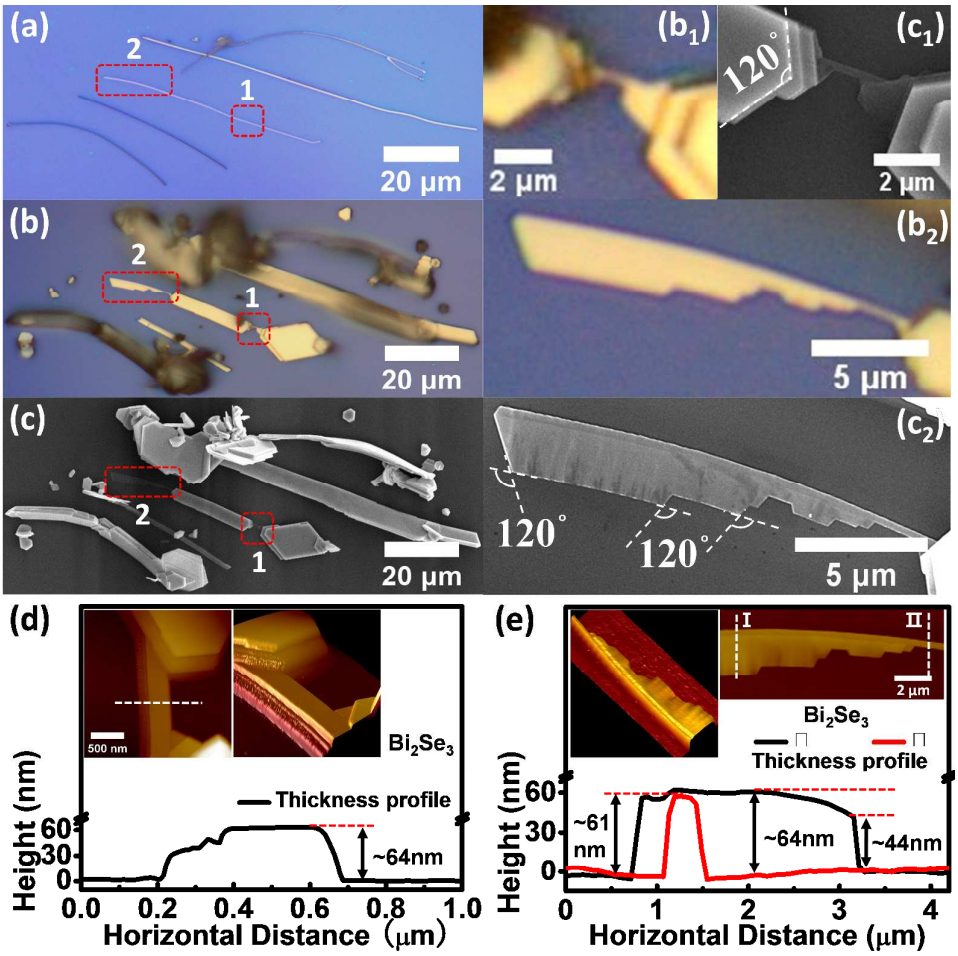

Figure 7. (a) Optical microscopy image of five nanoribbons, transferred mechanically for the first growth sample by micro-probe. (b) and (c) Optical microscopy and SEM images of the five nanoribbons after the secondary growth, respectively. (b_1) and (b_2) are the zoom-in optical microscopy images taken at the position 1 and 2 in (b), respectively. (c_1) and (c_2) are the zoom-in SEM images taken at the position 1 and 2 in (c), respectively. (d) and (e) are AFM images taken at the position 1 and 2, respectively. The thickness profiles were taken at the white dash lines, correspondingly.

Graphical Abstract

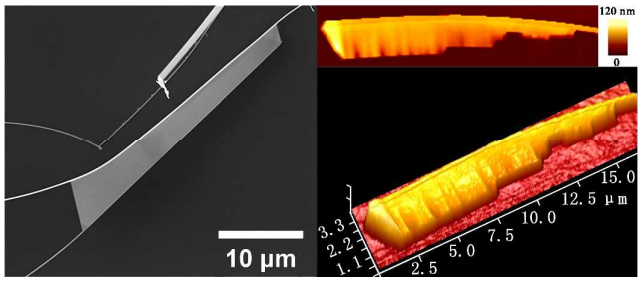

Typical bridge-like Bi_2Se_3 nanosturctures

"Two-step growth" method for obtaining large dimensional bridge-like Bi_2Se_3 nanostructures was proposed for the first time.